Mechanics of Materials 68 (2014) 228–236

Contents lists available at ScienceDirect

Mechanics of Materials

journal homepage: www.elsevier.com/locate/mechmat

Numerical modelling of ductile damage evolution in tensile and bending tests of timber structures

A. Khennane [a], M. Khelifa [b,*], L. Bleron [b], J. Viguier [b]

[a] School of Engineering and Information Technology, UNSW Canberra, Northcott Drive, ACT 2600 Canberra, Australia
[b] University of Lorraine, ENSTIB/LERMAB, 27 rue du Philippe Séguin, Epinal, France

ARTICLE INFO

Article history:
Received 13 April 2013
Received in revised form 15 August 2013
Available online 18 September 2013

Keywords:
Orthotropic
Elasticity
Plasticity
Isotropic hardening
Ductile damage
Tensile test

ABSTRACT

The characteristic values for strength and stiffness of all sorts of timber products are based on the assumption of a linear relation between stress and strain prior to failure and consequently verification of the load-bearing capacity of individual members in a construction is also based on a similar linear relation. Such an approach is very conservative and ill suited for performance-based design, which requires a full analysis of the structure with the possibility of moment and/or stress redistribution within parts of the structure. The development of material models that encompass the complex behaviour of wood is therefore necessary. The present work presents a model formulated within the frameworks of plasticity and continuum damage mechanics (CDM). It applies the classical flow theory of plasticity to formulate ductile failure of wood in compression and damage mechanics for the brittle failure modes. It takes into account the orthotropic elastic behaviour, the plastic anisotropic isotropic hardening, the isotropic ductile damage, and the large plastic deformations. The model was used to predict the initiation and growth of ductile damage in tensile and bending tests on different timbers types. Good agreement was found between the predictions of the model and the experimental results.

1. Introduction

Finite element analysis of timber structures has acquired great importance in recent years due to the short supply of wood and increasing environmental awareness among users and manufacturers. Nowadays most of timber used in the construction industry comes from sustainable softwood plantations. This type of timber has lower elastic and strength properties than its hardwood counterpart. As a result, new designs of timber structures need to be optimised not only for stiffness and strength but also for cost. The best way to achieve such outcomes is through the use of numerical simulation. Successful numerical simulations however require realistic constitutive models that encompass the complexities of wood as a material. Its anisotropic nature limits the applicability of analytical models. It is highly orthotropic with large ratios of mechanical properties and strength between the respective values parallel and transverse to the grain direction. Its failure in compression in the direction parallel to the grain is very different from that perpendicular to the grain. At angles to the grain between 10° and 45°, the failure modes are brittle due to the activated transverse tension and shear. However, as the angle increases, the failure modes shift from brittle to ductile with large deformations leading to the onset of micro-defects as voids and micro cracks as supported by experimental evidence on different wood species as reported in Poulsen (1998), Reiterer and Stanzl-Tschegg (2001), Sandhaas (2012). When these micro-defects initiate and grow inside the plastically deformed wood, the stress and strain fields are deeply modified, leading to significant modifications in the deformation process itself. The coalescence of these defects can lead to the initiation of macro cracks or damaged zones, inducing an irreversible damage.

* Corresponding author. Tel.: +33 (0) 3 29 29 61 18.
E-mail address: mourad.khelifa@univ-lorraine.fr (M. Khelifa).

0167-6636/$ - see front matter © 2013 Elsevier Ltd. All rights reserved.
http://dx.doi.org/10.1016/j.mechmat.2013.09.004

Yet this complex behaviour is seldom taken into account in standards of practice. For instance, in Eurocode 5 (1995) the characteristic values for strength and stiffness of all sorts of timber products are based on the assumption of a linear relation between stress and strain prior to failure and consequently verification of the load-bearing capacity of individual members in a construction is also based on a similar linear relation except for members subjected to compression loading, for which a nonlinear elastic-plastic computation may be used. The maximum stress a timber member can resist is a function of the deformation modes and takes the form of a relationship between the low and large strains. Hence, it is necessary that load levels everywhere remain within the limit strengths fixed by EC5 in order to avoid damage occurrence. Such an approach is very conservative and ill suited for performance-based design, which requires a full analysis of the structure with the possibility of moment and/or stress redistribution within parts of the structure. A material model capable of being used in performance-based design must encompass the complex behaviour of timber. The latter can only be captured through the use of multidimensional failure criteria. Because of the interactions between brittle and ductile failure modes, it is crucial to use coupled constitutive equations accounting for both non-linear isotropic hardening and isotropic ductile damage.

The development of such models however has been hampered by the lack of data. It was only until the mid 80's that data on the general effect of multi-axial state of stress were made available (Mackenzie-Helnwein et al., 2003). Nonetheless some notable efforts were made to model the generalised behaviour of wood; among them the use of fracture mechanics (Barrett et al., 1981; Smith et al., 2003; Vasic et al., 2005; Van der Put, 2007), plasticity (Mackenzie-Helnwein et al., 2003), and damage mechanics (Wittel et al., 2005; Qing and Mishnaevsky, 2011). However all of the approaches suffer from some drawbacks. Fracture mechanics based models are very complex and computationally very expensive because of the required model scale and mesh size. Plasticity on its own is not capable of capturing stiffness degradation. As to damage, it is not capable of capturing permanent plastic deformations. More recently (Schmidt and Kaliske, 2009) developed a material model based on a multi-surface plasticity formulation with anisotropic, moisture and temperature dependent yield surfaces and direction dependent post-failure behaviour to model the permanent deformations and cohesive elements to discretely model tension and shear cracks. This formulation however required the definition of an interface element formulation with traction separation law for wood.

In the present work, a material model which can be easily implemented in existing finite element software is presented. The model is capable of describing the complex behaviour of timber. It is formulated within the frameworks of plasticity and continuum damage mechanics (CDM). It applies classical flow theory of plasticity to formulate ductile failure of wood in compression and damage mechanics for the brittle failure modes. It takes into account the orthotropic elastic behaviour, the plastic anisotropic isotropic hardening, the isotropic ductile damage, and the large plastic deformations. The wood material is considered as a continuous medium. The macroscopic approach not only saves considerable CPU time, but most studies have shown that it can successfully estimate the states of stress and strain (Khelifa et al., 2007; Oudjene and Khelifa, 2009). Furthermore, a material model based on CDM and plasticity can be easily implemented as a subroutine in existing finite element software. The model is used to predict damage occurrences in tensile and bending tests.

2. Constitutive equations for wood including damage

Wood is a lignocellulosic material admitting cylindrical symmetry. The presence of growth rings, which are used to indicate the age, contributes to some material heterogeneity. Yet in the mechanics of continuous media, it is assumed continuous and macroscopically homogeneous. Hence based on the geometry of a log, a Cartesian coordinate system LRT is defined as shown in Fig. 1.

The material model uses the coordinate system shown on Fig 1, and is formulated within the framework of thermodynamics of irreversible processes with internal variables (Khelifa et al., 2007; Oudjene and Khelifa, 2009; Lemaitre and Chaboche, 1978; Lemaitre and Chaboche, 1985; Murakami, 1988; Saanouni et al., 1994).

The state relations are written as:

$$\underline{\sigma} = (1-D)\underline{\underline{\Lambda}} : \underline{\varepsilon}^e \quad \text{(Cauchy stress tensor)} \tag{1}$$

$$R = (1-D) \times Q \times r \quad \text{(Isotropic hardening stress)} \tag{2}$$

$$Y = \frac{1}{2}\underline{\varepsilon}^e : \underline{\underline{\Lambda}} : \underline{\varepsilon}^e \quad \text{(Isotropic damage driving force)} \tag{3}$$

where D represents the damage parameter, $\underline{\varepsilon}^e$ represents the elastic strain tensor, $\underline{\sigma}$ the Cauchy stress tensor; (R, r) two scalar variables representing the isotropic hardening stresses, Q the isotropic hardening modulus, and $\underline{\underline{\Lambda}} \equiv \Lambda_{ijkl}$ the fourth-order operator of the elastic properties given as:

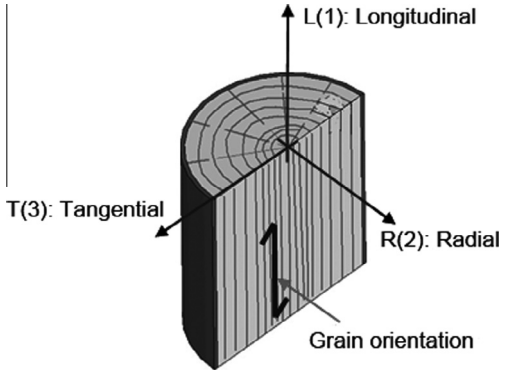

Fig. 1. LRT coordinate system for wood.

$$\begin{cases} \Lambda_{1111} = \frac{1-\nu_{23}\nu_{32}}{\Delta E_2 E_3}, \quad \Lambda_{2222} = \frac{1-\nu_{13}\nu_{31}}{\Delta E_1 E_3}, \quad \Lambda_{3333} = \frac{1-\nu_{12}\nu_{21}}{\Delta E_1 E_2}, \\ \Lambda_{1122} = \frac{\nu_{21}+\nu_{31}\nu_{23}}{\Delta E_2 E_3}, \quad \Lambda_{2233} = \frac{\nu_{32}+\nu_{12}\nu_{31}}{\Delta E_1 E_3}, \quad \Lambda_{1133} = \frac{\nu_{31}+\nu_{21}\nu_{32}}{\Delta E_2 E_3} \\ \Lambda_{1212} = 2G_{12}, \quad \Lambda_{2323} = 2G_{23}, \quad \Lambda_{1313} = 2G_{13}, \\ \Delta = \frac{1-\nu_{12}\nu_{21}-\nu_{23}\nu_{32}-\nu_{13}\nu_{31}-2\nu_{21}\nu_{32}\nu_{13}}{E_1 E_2 E_3} \end{cases} \tag{4}$$

where E_i (i=1,3) are the elastic modulii of the material along the directions shown in Fig. 1, ν_{ij} (i=1,3 ; j=1,3) are the Poisson's coefficients, and G_{ij} (i=1,3 ; j=1,3) the shear modulii.

The complementary relations are given as:

$$\dot{\underline{\varepsilon}}^{p} = \dot{\lambda}\frac{\underline{\underline{H}} : \underline{\sigma}}{\sqrt{1-D}\,\|\underline{\sigma}\|} = \dot{\lambda}\frac{\underline{n}}{\sqrt{1-D}} \quad \text{(Plastic strain rate tensor)} \tag{5}$$

$$\dot{r} = -\dot{\lambda}\left[\frac{1}{\sqrt{1-D}} - \mathrm{br}\right] \quad \text{(Isotropic hardening strain rate)} \tag{6}$$

$$\dot{D} = \dot{\lambda}\left(\frac{Y}{S}\right)^{s} \quad \text{(Isotropic damage rate)} \tag{7}$$

with:

$$\|\underline{\sigma}\| = \sqrt{\underline{\sigma} : \underline{\underline{H}} : \underline{\sigma}} \tag{8}$$

Where $\dot{\lambda}$ is the plastic multiplier, $\underline{n}$ is the normal to the loading surface, b is the non-linear isotropic hardening coefficient, s and S are the material coefficients describing the ductile damage evolution, $\|\underline{\sigma}\|$ is the norm of the Cauchy stress tensor in Hill's sense in which the symmetric fourth order tensor $\underline{\underline{H}} = H_{ijkl}$ is the classical Hill anisotropic tensor defining the initial plastic anisotropy, function of the six parameters F, G, H, L, M, and N, given as:

$$\begin{cases} H_{1111} = G+H, \quad H_{2222} = F+H, \quad H_{3333} = F+G, \\ H_{1122} = -H, \quad H_{2233} = -F, \quad H_{1133} = -G, \\ H_{1212} = 2N, \quad H_{2323} = 2M, \quad H_{1313} = 2L \end{cases} \tag{9}$$

The quadratic Hill yield criterion (Hill, 1948) accounting for the isotropic hardening and damage is written as:

$$f = \frac{\|\sigma\| - R}{\sqrt{1-D}} - \sigma_{\text{yield}} \leqslant 0 \tag{10}$$

in which σ_{yield} is the limit yield stress in uniaxial tension i.e., the initial size of the yield surface in the stress space.

The model evolved from a previous one developed for anisotropic plasticity in metals (Khelifa et al., 2007). Unlike metal plasticity, the model does not account for kinematic hardening; the parameters Q and b suffice to describe the isotropic hardening. In addition, the damage can be characterised by only two parameters, S and s. In Eq. (7), the parameter S account for the ductility of the material, and the exponent s is used to accelerate or delay the occurrence of damage. In the absence of damage, the above equations reduce to classical elastoplastic constitutive equations. They are implemented into the ABAQUS/Explicit (Systèmes) FE software thanks to the Vumat user subroutine as will be discussed hereafter.

3. Numerical implementation

Using a Dynamic Explicit scheme (DE), the constitutive equations are integrated over a time increment to obtain the quantities $\underline{\sigma}_{n+1}$, R_{n+1} and D_{n+1}. The tensor of plastic strains $\underline{\varepsilon}^{p}_{n+1}$ and the damage parameter D_{n+1} are obtained using the θ-method while the isotropic hardening variable is r_{n+1} is obtained with the asymptotic method; that is:

$$\underline{\varepsilon}^{p}_{n+1} = \underline{\varepsilon}^{p}_{n} + \frac{\Delta\lambda}{\sqrt{1-D_{n+1}}}\underline{n}_{n+1} \tag{11}$$

$$D_{n+1} = D_n + \Delta\lambda\left[\frac{Y_{n+1}}{S}\right]^{s} \tag{12}$$

$$r_{n+1} = r_n e^{-b\Delta\lambda} + \frac{(1-e^{-b\Delta\lambda})}{b\sqrt{1-D_{n+1}}} \tag{13}$$

The plastic criterion, f_{n+1}, which should satisfy the consistency condition at time t_{n+1} is given as:

$$f_{n+1} = \frac{\|\underline{\sigma}_{n+1}\| - R_{n+1}}{\sqrt{1-D_{n+1}}} - \sigma_{\text{yield}} = 0 \tag{14}$$

Given a total strain increment $\Delta\underline{\varepsilon}$ at time t_n, assuming the response to be initially elastic, the trial stress at time t_{n+1} is obtained as:

$$\underline{\sigma}^{*}_{n+1} = \underline{\sigma}_n + (1-D_n)\underline{\underline{\Lambda}} : \Delta\underline{\varepsilon} \tag{15}$$

which is then substituted in the expression of the failure criteria to yield:

$$f^{*}_{n+1} = \frac{\|\underline{\sigma}^{*}_{n+1}\| - R_n}{\sqrt{1-D_n}} - \sigma_{\text{yield}} \tag{16}$$

$$\text{with } \|\underline{\sigma}^{*}_{n+1}\| = \sqrt{\underline{\sigma}^{*}_{n+1} : \underline{\underline{H}} : \underline{\sigma}^{*}_{n+1}} \tag{17}$$

If $f^{*}_{n+1} < 0$, the obtained response is elastic, and the tensorial quantities at time t_{n+1} are obtained as:

$$\underline{\sigma}_{n+1} = \underline{\sigma}^{*}_{n+1}, R_{n+1} = R_n \quad \text{and} \quad D_{n+1} = D_n \tag{18}$$

Otherwise, if $f^{*}_{n+1} \geqslant 0$, it becomes necessary to apply a correction to the trial stresses $\underline{\sigma}^{ast}_{n+1}$ to obtain $\underline{\sigma}_{n+1}$, R_{n+1} and D_{n+1} such that:

$$f_{n+1} = \frac{\|\underline{\sigma}_{n+1}\| - R_{n+1}}{\sqrt{1-D_{n+1}}} - \sigma_{\text{yield}} = 0 \tag{19}$$

with:

$$\|\underline{\sigma}_{n+1}\| = \sqrt{\underline{\sigma}_{n+1} : \underline{\underline{H}} : \underline{\sigma}_{n+1}} \tag{20}$$

$$\underline{\sigma}_{n+1} = \underline{\sigma}^{*}_{n+1} - (1-D_{n+1})\underline{\underline{\Lambda}} : \Delta\underline{\varepsilon}^{p} \tag{21}$$

$$\Delta\underline{\varepsilon}^{p} = \frac{\Delta\lambda}{\sqrt{1-D_{n+1}}}\underline{n}_{n+1} \tag{22}$$

$$R_{n+1} = Q(1-D_{n+1})\left(r_n e^{-b\Delta\lambda} + \frac{(1-e^{-b\Delta\lambda})}{b\sqrt{1-D_{n+1}}}\right) \tag{23}$$

$$Y_{n+1} = \frac{1}{2}\frac{\underline{\sigma}_n : \underline{\underline{\Lambda}}^{-1} : \underline{\sigma}_n}{(1-D_{n+1})^2} + \frac{1}{2}\left(\Delta\underline{\varepsilon} - \Delta\lambda\frac{\underline{n}_{n+1}}{\sqrt{1-D_{n+1}}}\right) : \underline{\underline{\Lambda}} : \left(\Delta\underline{\varepsilon} - \Delta\lambda\frac{\underline{n}_{n+1}}{\sqrt{1-D_{n+1}}}\right) + \frac{\underline{\sigma}_n}{(1 - D_{n+1})} : \left(\Delta\underline{\varepsilon} - \Delta\lambda\frac{\underline{n}_{n+1}}{\sqrt{1-D_{n+1}}}\right) \quad (24)$$

The final system of equations to solve then becomes:

$$\begin{cases} f_{n+1}(\Delta\lambda, \underline{n}_{n+1}, D_{n+1}) = \frac{\|\underline{\sigma}_{n+1}\| - R_{n+1}}{\sqrt{1-D_{n+1}}} - \sigma_{yield} = 0 \\ \underline{h}_{n+1}(\Delta\lambda, \underline{n}_{n+1}, D_{n+1}) = \underline{\underline{H}} : \underline{\sigma}_{n+1} - \|\underline{\sigma}_{n+1}\|\underline{n}_{n+1} = 0 \\ g_{n+1}(\Delta\lambda, \underline{n}_{n+1}, D_{n+1}) = D_{n+1} - D_n - \Delta\lambda\left[\frac{Y_{n+1}}{S}\right]^s = 0 \end{cases} \quad (25)$$

The tensorial function $\underline{h}_{n+1}$ stems from the normality rule to the loading surface, and g_{n+1} is a scalar function, which governs damage. The variables $\Delta\lambda$, $\underline{n}_{n+1}$ and D_{n+1} are the unknowns. The solution of the system is obtained with the Newton–Raphson method.

The finite element method is used to discretise the global equilibrium equation expressed as follows:

$$[M]\{\ddot{U}\} + \{R\} = 0; \{R\} = \{F\}_{int} - \{F\}_{ext} \quad (26)$$

where $[M]$ is the mass matrix, $\{\ddot{U}\}$ is the acceleration vector, $\{R\}$ is the residual pseudo-load vector, $\{F\}_{int}$ the internal load vector and $\{F\}_{ext}$ the external load vector.

The system of Eq. (26) is solved with the help of the explicit algorithm, which consists in obtaining a solution at the instant t_{n+1} based on known quantities at the instant t_n:

$$\{\ddot{U}\}_n = [M]^{-1}\{R\}_n \quad (27)$$

$$\{\dot{U}\}_{n+1/2} = \{\dot{U}\}_{n-1/2} + \frac{\Delta t^{n+1} + \Delta t^n}{2}\{\ddot{U}\}_n \quad (28)$$

$$\{U\}_{n+1} = \{U\}_n + \Delta t_{n+1}\{\dot{U}\}_{n+1/2} \quad (29)$$

where $\{\ddot{U}_n\}$ is the acceleration vector at time t_n, $\{\dot{U}_{n+1/2}\}$ is the velocity vector at half step, and $\{U_{n+1}\}$ is the displacement vector at time t_{n+1}. The stability and precision of an explicit scheme depends very much on the chosen time increment. An estimate of a stable time increment is obtained as follows:

$$\Delta t = \min\left[\frac{L_e}{c_d}\right] \quad (30)$$

where L_e represent the characteristic length of the smallest element, c_d is the dilatational wave speed, which in turn is given as:

$$c_d = \sqrt{\frac{E}{\rho}} \quad (31)$$

ρ is the material density, E is the Young's moduli.

The material model is implemented in Abaqus Explicit using a VUMAT user defined subroutine (Dassault Systèmes)

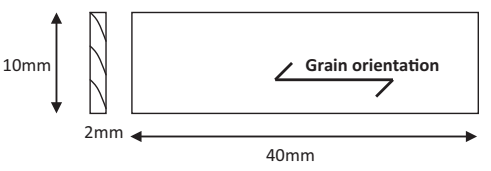

(a). Geometry of the specimen in tension

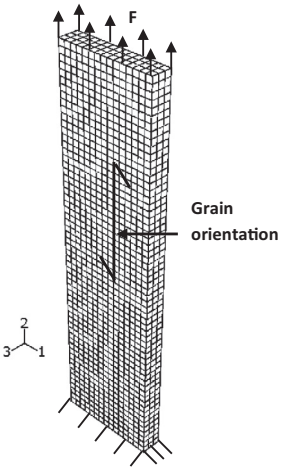

(b). FE model

Fig. 2. Tensile test (geometry, mesh and boundary conditions).

Table 1
Material properties for pine wood.

Elasticity	E_1 = 13.01 GPa	$E_2 = E_3$=0.87 GPa	$\nu_{12} = \nu_{13}$ = 0.29	$\nu_{23} = \nu_{32}$ = 0.02
	$G_{12} = G_{LT}$ = 0.98 GPa	G_{23}=0.34 GPa		
Plasticity	σ_{yield} = 43.1 MPa	Q = 130 MPa ; b = 21	$F = G = H$ = 0.5 ; $L = M = N$ = 1.5	
Damage	S = 0.051 MPa	s = 1.5		

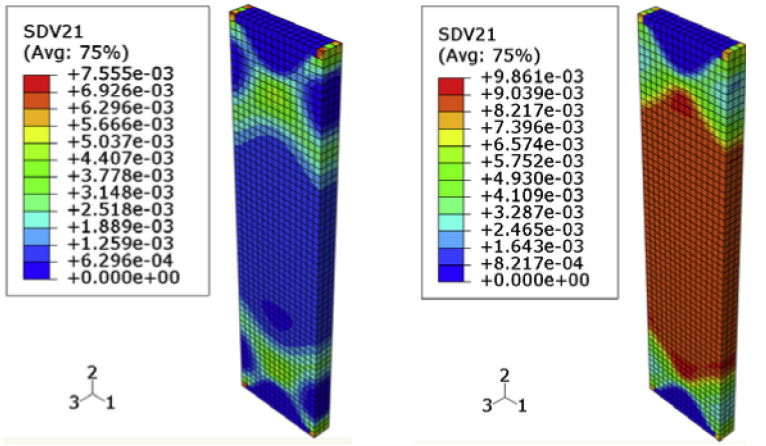

(a) v=0.015mm

(b) v=0.096mm

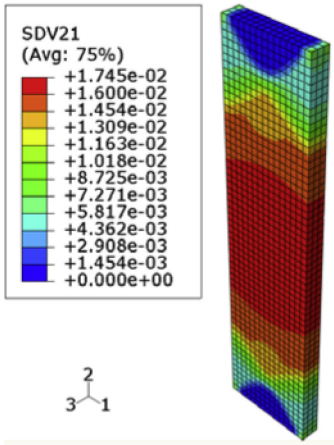

(c) v=0.141mm

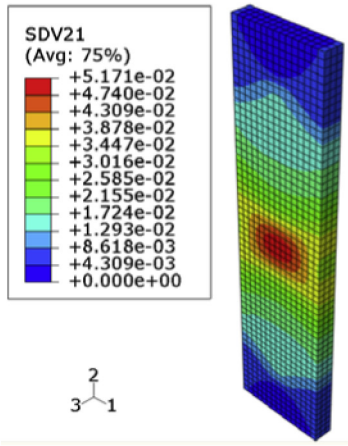

(d) v=0.177mm

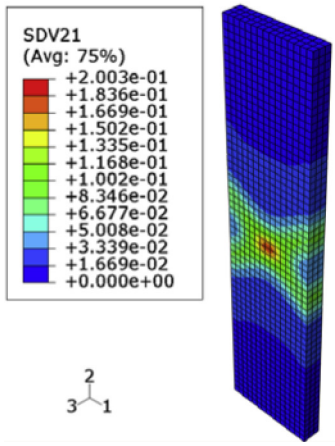

(e) v=0.184mm

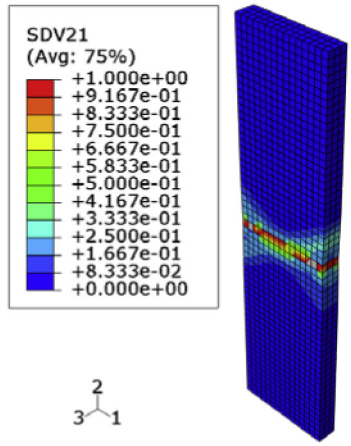

(f) v=0.2mm

Fig. 3. Damage distribution at different displacement values.

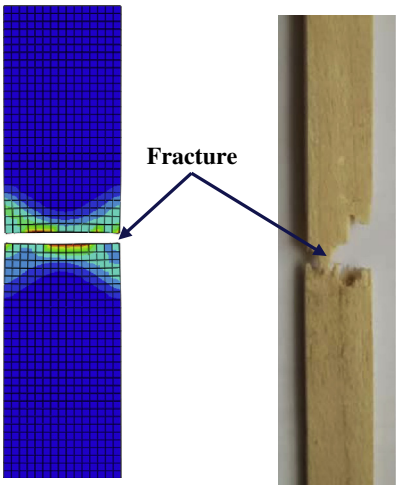

Fig. 4. Fracture in tensile test (simulation and experiment).

4. Results and discussions

4.1. Tensile test

The tensile test consists of a specimen of pine wood whose geometric characteristics are shown on Fig. 2. The analysis focuses on the middle part of the specimen far from the stress concentration zones caused by the boundary conditions. The specimen is meshed with the C3D8R element available in the ABAQUS/Explicit library. It is an 8-node hexahedral brick element with reduced integration. The loading is applied in the form of an imposed displacement at a rate of 1mm/min. The density of the wood is taken equal to 460 kg/m^3, and the material properties are listed in Table 1.

Fig. 3 shows the evolution of damage in the form of contour plots at various displacements, $v = 0.015$ mm, 0.096 mm, 0.141 mm, 0.177 mm, 0.184 mm and at rupture. It appears clearly that there are three stages of damage. For displacements less than $v = 0.096$ mm, the damage distribution is homogeneous as shown on Fig. 1a and b. Beyond this limit, the damage becomes heterogeneous. A highly strained zone appears in the middle of the specimen at a displacement of $v = 0.177$ mm (Fig. 3c and d). This is followed by the quick formation of two shear bands, before a macroscopic crack starts at the intersection of the two bands at a displacement of $v = 0.184$ mm. It can be seen that the rupture facies is perpendicular to the longitudinal axis of the sample. The damage reaches the maximum value $D = 1$ in the cracked zones (Fig. 3f).

Fig. 4 shows a comparison between the predicted rupture and the experimental one. It is interesting to note that the model accurately predicts the emplacement of the damaged zone, which corresponds exactly to the specimen failure.

The obtained results are also reported in the form of load–displacements curves with some deformed configurations of the specimen as shown in Fig. 5. It can be seen that the predicted response is in good agreement with the experiment. From Fig. 5, one can observe the strong effect of softening induced by the damage occurrence. The maximum predicted load carrying capacity of the

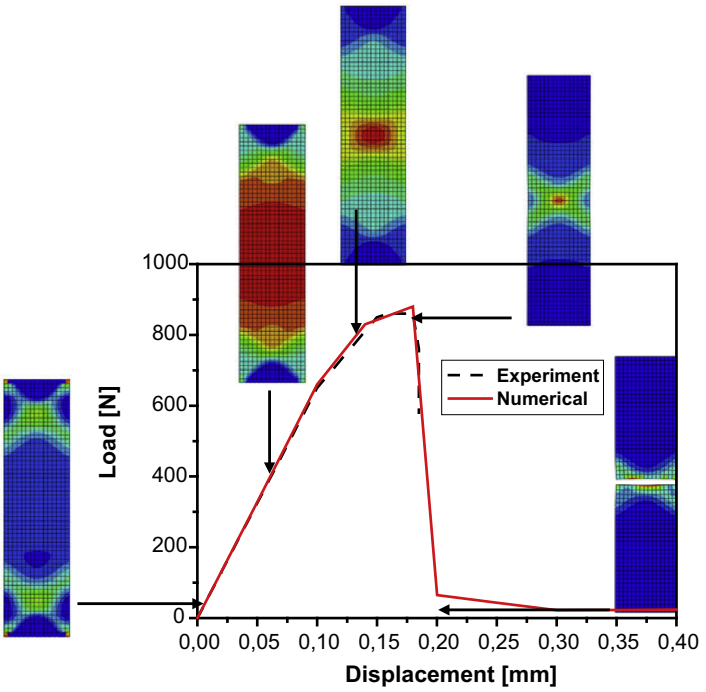

Fig. 5. Force versus displacement curves (tensile test).

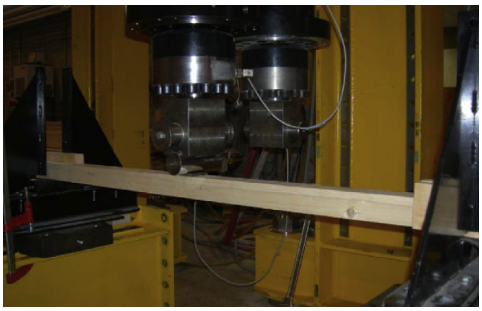

(a) 3-points bending test specimen

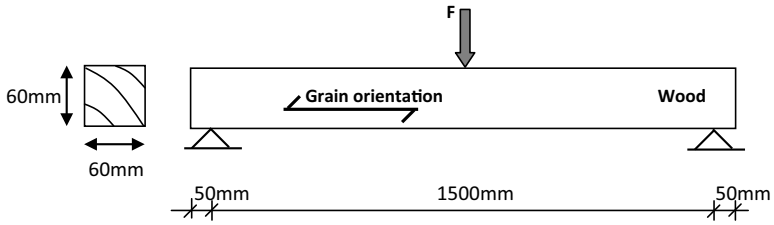

(b) Specimen geometry

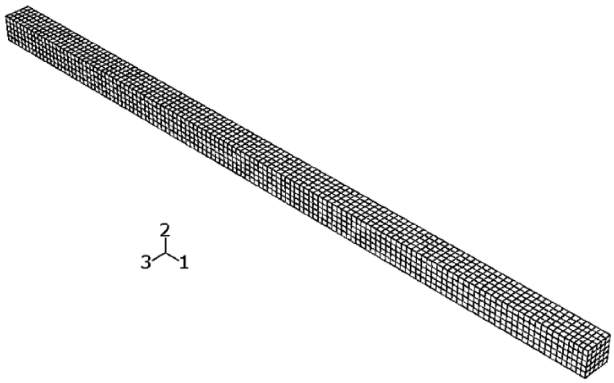

(c) FE Model

Fig. 6. Three-points bending test.

Table 2
Material properties for spruce wood.

Elasticity	E_1 = 13.5 GPa	$E_2 = E_3$ = 1.8 GPa	$\nu_{12} = \nu_{13}$ = 0.29	$\nu_{23} = \nu_{32}$ = 0.02
	$G_{12} = G_{LT}$ = 0.9 GPa	G_{23} = 0.37 GPa		
Plasticity	σ_{yield} = 35.1MPa	Q = 150 MPa ; b = 13	$F = G = H$ = 0.5 ; $L = M = N$ = 1.5	
Damage	S = 0.01 MPa	s = 1		

specimen, F_{max} = 867.43 N, is reached at a displacement of v = 0.177 mm. This is just slightly over the experimental one, which is equal to F_{max} = 853.67 N. It is interesting to note that the specimen reaches its limit capacity only after undergoing some nonlinear response. It is very clear that the standards of practice, which use strength and stiffness values based on the assumption of a linear relation between stress and strain, are very conservative.

4.2. Bending test

Fig. 6 shows a beam sample made of spruce wood subject to a three bending test. The three points bending test is used in practice to measure the ultimate strength of timber. The experimental set up, the geometric characteristics of the sample, and the FE mesh used for the model are shown in Fig. 6a–c respectively.

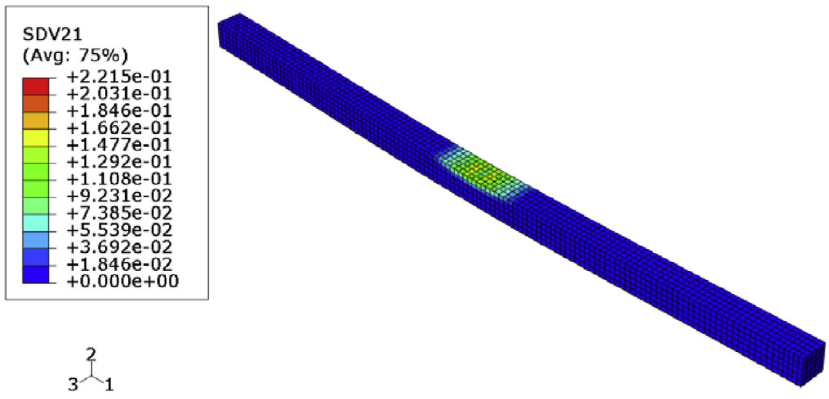

(a). v=24.96mm

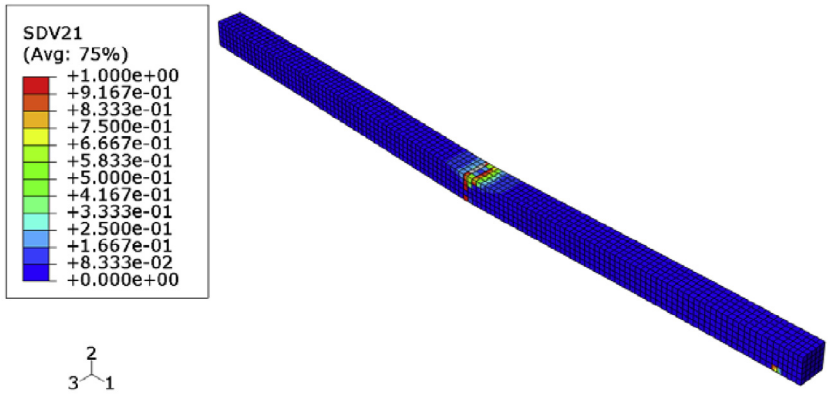

(b). v=25.5mm

Fig. 7. Damage distribution at different displacement values.

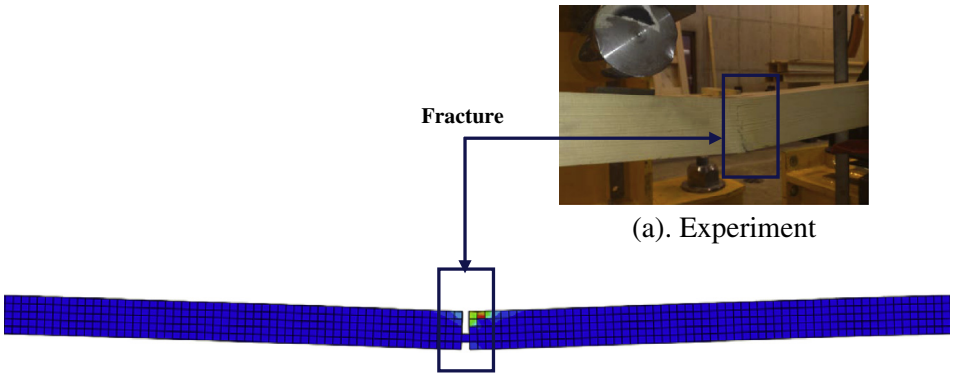

(a). Experiment

(b). Numerical

Fig. 8. Fracture in bending test (simulation and experiment).

As for the uniaxial test, the 8-node hexahedral brick element with reduced integration C3D8R is used for the mesh. The different material properties and parameters for the spruce wood are listed in Table 2.

Fig. 7 shows the damage evolution in the sample. The first damage occurs in the vicinity of the loading region (Fig. 7a). As the load increases, the damaged zone quickly increases in intensity. A strong localization of damage is

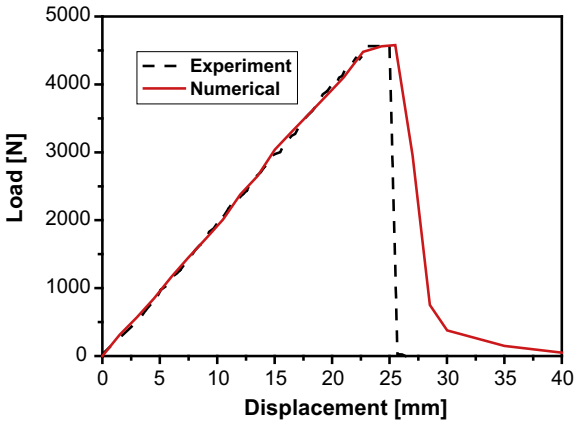

Fig. 9. Force versus displacement curves (bending test).

induced at a displacement of $v = 24.96$ mm. This quickly transforms into macroscopic cracks, and failure occurs in a catastrophic manner at a displacement of $v = 25.5$ mm.

Fig. 8 shows a comparison between the experimental rupture and that predicted using the developed model. The computed ultimate load at failure $F_{max} = 4.58$ kN is almost identical to the experimental one, $F_{max} = 4.51$ kN (Fig. 9). The computed displacement $v = 25.5$ mm at failure is in good agreement with the experimental value $v = 25.6$ mm.

5. Conclusion

A three-dimensional constitutive model for wood suitable for performance based analysis of timber structures is presented. The model is based on the thermodynamics of irreversible processes. The model uses damage mechanics and plasticity to account respectively for stiffness degradation and permanent plastic deformations, and was successfully implemented in ABAQUS/Explicit. It was shown that the model is capable of predicting the onset of macroscopic fractures in timber specimen during tensile and bending tests. In particular it was found that under uni-axial conditions, spruce wood undergoes nonlinear deformations before reaching its limit strength, which so far has been overlooked in standards of practice.

Further work is of course still needed in order to improve the capabilities of this model; in particular, the addition of damage induced anisotropy and moisture effects.

References

Barrett, J.D., Haigh, I.P., Lovegrove, J.M., 1981. Fracture mechanics and the design of wood structures. Philos. Trans. R. Soc. London A299, 217–226.

Dassault Systèmes, "ABAQUS Documentation Version 6.10, http://www.simulia.com/".

Eurocode 5, "Design of timber structures", 1995.

Hill, R. 1948. A theory of yielding and plastic flow of anisotropic metals. R. Soc. London Proc. p. 281.

Khelifa, M., Oudjene, M., Khennane, A., 2007. Fracture in sheet metal forming: effect of ductile damage evolution. Comput. Struct. 85 (3-4), 205–212.

Lemaitre, J., Chaboche, J.-L., 1978. Aspects phénoménologiques de la rupture par endommagement. J. Mech. Appl. 2 (3), 317–365.

Lemaitre, J., Chaboche, J.-L., 1985. Mécanique des matériaux solides. Dunod, Paris.

Mackenzie-Helnwein, P., Eberhardsteiner, J., Mang, H.A., 2003. A multi-surface plasticity model for clear wood and its application to the finite element analysis of structural details. Comput. Mech. 31, 204–218.

Murakami, S., 1988. Mechanical modeling of material damage. J. Appl. Mech. 55, 280–286.

Oudjene, M., Khelifa, M., 2009. Finite element modelling of wooden structures at large deformations and brittle failure prediction. Mater. Des. 30 (10), 4081–4087.

Poulsen, J.S. 1998. Compression in Clear Wood. PhD thesis, Technical University of Denmark.

Qing, H., Mishnaevsky Jr, L., 2011. A 3D multilevel model of damage and strength of wood: analysis of microstructural effects. Mech. Mater. 43, 487–495.

Reiterer, A., Stanzl-Tschegg, S.E., 2001. Compressive behaviour of softwood under uniaxial loading at different orientations to the grain. Mech. Math. 33, 705–715.

Saanouni, K., Forster, C., BenHatira, F., 1994. On the anelastic flow with damage. Int. J. Damage Mech 3, 141–169.

Sandhaas, C. 2012. Mechanical Behaviour of Timber Joints with Slotted-in Steel Plates, PhD thesis, Delft University of Technology.

Schmidt, J., Kaliske, M., 2009. Models for numerical failure analysis of wooden structures. Eng. Struct. 31, 571–579.

Smith, I., Landis, E., Gong, M., 2003. Fracture and Fatigue in Wood. Wiley, Chichester.

Van der Put, T.A.C.M., 2007. A new fracture mechanics theory for orthotropic materials like wood. Eng. Fract. Mech. 74, 771–781.

Vasic, S., Smith, I., Landis, E., 2005. Finite element techniques and models for wood fracture mechanics. Wood Sci. Technol. 39, 3–17.

Wittel, F.K., Dill-Langer, G., Kroplin, B.H., 2005. Modeling of damage evolution in soft-wood perpendicular to grain by means of a discrete element approach. Comput. Mater. Sci. 32, 594–603.